Optics & Laser Technology 158 (2023) 108818

Contents lists available at ScienceDirect

Optics and Laser Technology

journal homepage: www.elsevier.com/locate/optlastec

Full length article

Compact, repetition rate locked all-PM fiber femtosecond laser system based on low noise figure-9 Er:fiber laser

Haihao Cheng [a,b], Zhao Zhang [a,b], Ran Pan [a,b], Ting Zhang [a,b], Ye Feng [a], Xiaohong Hu [a,*], Yishan Wang [a,b], Shun Wu [a,c]

[a] State Key Laboratory of Transient Optics and Photonics, Xi'an Institute of Optics and Precision Mechanics, Chinese Academy of Sciences, Xi'an 710119, China
[b] University of Chinese Academy of Sciences, Chinese Academy of Sciences, Beijing 100049, China
[c] Hubei Key Laboratory of Optical Information and Pattern Recognition, Wuhan Institute of Technology, Wuhan 430205, China

ARTICLE INFO

Keywords:
Figure-9 all-PM fiber laser
Amplitude noise and timing jitter
Femtosecond pulse amplification and compression
Polarization-maintaining

ABSTRACT

We demonstrate a compact femtosecond fiber laser system based on all polarization-maintaining (PM) fiber and fiber components integrated structure. The figure-9 oscillator which incorporated a nonlinear amplifying loop mirror in the cavity features a 103.4-MHz high repetition rate with up to 93.1 dB signal-to-noise ratio of the radio frequency spectrum, 0.0056% [1 Hz, 1 MHz] integrated root-mean-square amplitude noise at the fundamental repetition rate and 63.7-fs timing jitter [100 Hz, 1 MHz]. Meanwhile, the fundamental repetition frequency was also locked to a stable radio frequency reference by using a self-designed frequency actuator and a relative frequency stability of 2.1×10^{-12} at 1-s gate time was obtained. Moreover, benefitting from the large positive group-velocity dispersion and negative third-order dispersion at 1.5-μm wavelength band, we also achieved 48.2 fs compressed pulse duration as well as an amplified average power of 199 mW via one-stage all-PM fiber amplifier and compressor. At last, as a performance proof, by directly splicing 38-cm long PM highly nonlinear fiber to the pulse compressor, a broadband coherent supercontinuum spanning from 950 nm to 2150 nm was generated. Our all-PM fiber laser system is suitable for the further buildup of a low noise PM fiber optical frequency comb.

1. Introduction

In recent years, with the significant progress of fiber laser and amplifier, the ultrafast femtosecond laser systems with high average powers play a critical role in many applications such as high precision machining [1,2], clinical surgery [3,4], optical frequency comb (OFC) [5,6], high-harmonic generation [7,8], attosecond science [9,10], supercontinuum (SC) [11] and so on. For instance, in the process of SC generation, femtosecond pulses with a pulse duration of usually shorter than 100 fs and a peak power of 10 kW level are adopted to pump a short piece of highly-nonlinear fiber (HNLF) [11], a broadband coherent SC with low intensity noise can then be generated [12]. Generally speaking, an ultrashort pulse fiber laser system consists of a mode-locked fiber oscillator and the subsequent pulse amplification and compression modules. The noise property of the oscillator has a pivotal role in the noise performance of the whole system. According to the research results, we know that the shorter the pulse width, the higher the pulse energy can lead to much lower timing jitter level of the output laser pulse train [13]. The dispersion effects on the performances of the fiber lasers have also been studied [14–17]. In 2011, Lora Nugent-Glandorf et al. experimentally demonstrated that, for a stretched-pulse Yb:fiber oscillator with a near zero cavity dispersion, a reduced relative intensity noise (RIN), narrowest linewidth of the carrier-envelope offset (CEO) frequency (f_{ceo}) and less f_{ceo} frequency noise could be obtained [14]. In the same year, Youjian Song et al. further studied the impact of pulse dynamic on timing jitter of nonlinear polarization evolution (NPE) mode-locked Yb: fiber lasers. The quantum-limited timing jitter spectra over the full Nyquist frequency of soliton, stretched pulse and self-similar regimes were all characterized by using the balanced optical cross-correlation (BOC) method. It was indicated that, for a near zero cavity dispersion or stretched pulse operation, the smallest integrated root-mean-square (rms) timing jitter could be obtained. More importantly, the research results showed that, in addition to the intracavity dispersion, the pulse dynamic could also significantly affect the timing jitter spectrum and, in soliton regime with relatively high negative intracavity dispersion, an amplified spontaneous emission (ASE)

* Corresponding author.
E-mail address: xhhu@opt.ac.cn (X. Hu).

https://doi.org/10.1016/j.optlastec.2022.108818
Received 1 June 2022; Received in revised form 22 September 2022; Accepted 18 October 2022
Available online 26 October 2022

quantum-noise-limited timing jitter comparable to the one in stretched-pulse regime could also be realized [15]. In 2021, Łaszczych et al. characterized the output spectra and power under different net intracavity dispersion [16]. The net dispersion ranging from -0.065 ps^2 to $+0.038$ ps^2 was tailored by using a Martinez-type compressor. The experimental results showed that the broadest spectra could be realized by tailoring the net cavity dispersion to near zero. Meanwhile, in both the soliton and dissipative soliton regimes, for a constant pump power, when the net dispersion was varied, mode locking states with slightly different output power could be obtained. In 2020, Mayer et al. systematically studied five mode-locked states of an all polarization maintaining (PM) nonlinear amplifying loop mirror (NALM) Yb:fiber laser by incorporating a grating pair, three waveplates and a Faraday rotator in the oscillator cavity [17]. The mode-locked spectra, radio frequency spectra, RIN, phase noise/timing jitter and linewidths of the free running CEO frequency corresponding to net intracavity dispersion values ranging from -0.035 ps^2 to $+0.015$ ps^2 were all carefully characterized. The research results showed that, restricted by the soliton effects, the spectral width was narrow (e. g., smaller than 10 nm) when the central wavelength located in the anomalous dispersion region. A broader spectral width together with a higher output power could be realized when the central wavelength lay in the near-zero and normal dispersion region. Moreover, when the laser operated in the close to zero dispersion regime, much smaller RIN and timing jitter values could be obtained.

Because of the replacement of the external modulation elements necessary for the active mode-locking lasers and the real saturable absorbers often used in the passive mode-locking lasers, the lasers mode-locked based on unbalanced nonlinear process resulted artificial fast saturable effect can operate in low noise states together with simple and compact structures. Up to now, three most popular artificial saturable absorbers named nonlinear polarization rotation (NPR) or NPE [18–23], nonlinear optical loop mirror (NOLM) and NALM [24–26] are used to fabricate mode-locked fiber lasers. All of these mechanisms could help to generate sub-picosecond laser pulses. However, NPR and NPE rely on the polarization effect of the fiber and thus are sensitive to various kinds of environmental perturbations. This is the main reason why this kind of lasers are not proper for the outdoor applications. Instead, when the NOLM and NALM mode-locked fiber lasers are designed with an all-PM structure, the stabilities can be greatly improved. In 2016, N. Kuse et al. firstly demonstrated an 83-MHz fully stabilized all-PM Er:fiber OFC with a NALM [27]. The linear arm part of the figure-9 oscillator consisted of a spatially coupled graphene modulator and a bulk electro-optic modulator. These modulators were adopted to realize a fast control of the f_{ceo} and optical beat frequency (f_{beat}). A piezoactuator transducer (PZT) was attached to a fiber in the NALM loop for slow control of f_{beat}. The linear arm and NALM loop were bridged through a 2×2 fiber coupler with a splitting ratio of 50:50. Few milliwatts femtosecond mode-locked pulses were delivered through one port of the fiber coupler. In 2017, W. Hänsel et al. reported on a novel architecture of figure-9 fiber laser with a nonreciprocally biased NALM [28]. The nonreciprocal beam splitter and phase shifter (PS) in the linear arm part of the laser was constructed by the bulk components including two polarizing beam splitters (PBSs), a 45° Faraday rotator and a waveplate. Based on this configuration, the splitting ratio could be fine-tuned away from 50:50 while keeping the maximum round-trip transmission unchanged. Mode-locked femtosecond fiber lasers operating at wavelengths of 1030, 1565, and 2050 nm were demonstrated by using the designed laser structure. Especially, at 1565-nm wavelength, a high repetition rate of 250 MHz, together with 43-nm spectral bandwidth was obtained benefiting from the compact optical path of the linear arm and near to zero net cavity dispersion. In 2017, an all-PM fiber integrated, NALM mode-locked Er:fiber laser with a fundamental repetition rate of 48.8 MHz-64.7 MHz was first reported. A $\pi/2$ non-reciprocal PS was adopted in the NALM loop [29]. In 2019, Ke Yin et al. further proposed an optimal structure of NALM mode-locked Er:fiber laser and realized 477-fs output pulse duration and 121-MHz repetition rate [30]. In 2020, Yue Zhou et al. used a spool of PM dispersion-compensating fiber (DCF) to manage the intracavity dispersion and obtained stretched pulse mode locking with a repetition rate of ~40 MHz [31]. In 2021, Qinghui Deng et al. further adopted a homemade hybrid component which integrated the functions of PS and wavelength division multiplexer (WDM) to realize an all-PM figure-9 Er:fiber laser with a repetition rate up to 201.14 MHz [32]. However, most of the above research works focused only on the build-up of the mode-locked fiber oscillator. In 2021, Yuxuan Ma et al. designed and demonstrated a compact, robust, all-PM-fiber integrated 1.03 μm Yb:fiber laser mode-locked by NALM [33]. A chirped fiber Bragg grating (CFBG) with high peak transmittance of 80% and negative dispersion was used to achieve high output power and manage the net intracavity dispersion to -0.01 ps^2. The effects of the cavity parameters including the phase bias, power splitting ratio of the 2×2 coupler, fiber asymmetry in the NALM loop and bandwidth of the CFBG on the initiation of mode locking and laser output properties were numerically studied. The laser delivered 54 MHz mode-locked pulses with an average power up to 51 mW. In addition, the laser showed an integrated RIN of 0.0255% [10 Hz, 1 MHz] and the rms timing jitter of 0.7 fs [25 kHz, 5 MHz] measured by the BOC method. The pump noise together with the high cavity output ratio resulted low cavity-Q should be responsible for the relative high RIN.

From the perspective of practical and outdoor applications, the boost of the average power through a high-performance all fiber amplifier is also critical. The universal amplification techniques include chirped-pulse amplification (CPA) [34,35] and nonlinear pulse amplification (NPA) [36,37]. The main difference is that the nonlinear phase accumulation in CPA scheme is avoided while in NPA scheme, it should be carefully designed. Moreover, the NPA system usually needs a pulse pre-shape structure to manage the group-velocity dispersion (GVD) and third-order dispersion (TOD) or to provide adaptive nonlinearity, so the amplified pulse can then be compressed by a CFBG or simply by a segment of single-mode fiber (SMF) with a proper length and an all-fiber structure can then be completed [38]. In 2015, D. G. Purdie et al. reported an erbium-doped fiber (EDF) amplifier which was characterized by the adoption of non-PM DCF as the dispersion management component. The oscillator delivered mode-locked pulses with a repetition rate of 18.67 MHz. Mode-locked operation of the fiber ring laser was achieved based on a graphene saturable absorber. The seed pulses output from the oscillator were pre-stretched by a piece of non-PM DCF. 29-fs compressed pulse duration and ~52 mW amplified average output power corresponding to 2.8-nJ single pulse energy were realized [39]. In 2016, Jia Yu et al. presented an all-PM fiber based NPA system. The system included a semiconductor saturable-absorber mirror assisted 200-MHz mode-locked fiber laser, two-stage EDF amplifiers and the subsequent PM-SMF compressor. The first stage of the amplifier mainly functioned as a pulse stretcher and the second-stage amplifier was then used to boost the average power. 34-fs compressed pulse duration and 320-mW average power corresponding to 1.6-nJ pulse energy were obtained [40]. In 2017, Hao Luo et al. exhibited a non-PM EDF based all fiber laser system and obtained 120-mW amplified average power, 2.8-nJ single pulse energy and 22.7-fs compressed pulse duration. 44.6-MHz seed pulses with single pulse duration of 1.5 ps from a ring cavity fiber oscillator mode-locked by NPR effect were first pre-chirped by 4.62-m long standard non-PM SMF before amplification [41]. In 2017, starting from all-PM NALM mode-locked Er:fiber lasers with fundamental repetition rates of 48.8 MHz and 64.7 MHz, Feihong Chen et al. achieved 28-fs compressed pulse duration and 172-mW amplified average power [29]. In 2019, Zhengru Guo et al. designed 1.84-MHz low repetition rate all PM fiber amplifier based on figure-9 mode-locked laser. In their works, a reflection-type PS was used and the Kelly sidebands were partially filtered by a 6.4-nm filter. By coupling the filtered seed pulses into a piece of Er-Yb-codoped fiber, the average power was boosted to 2.8 W, yielding a pulse energy of 1.5 μJ with the pulse duration of 51 ps [42].

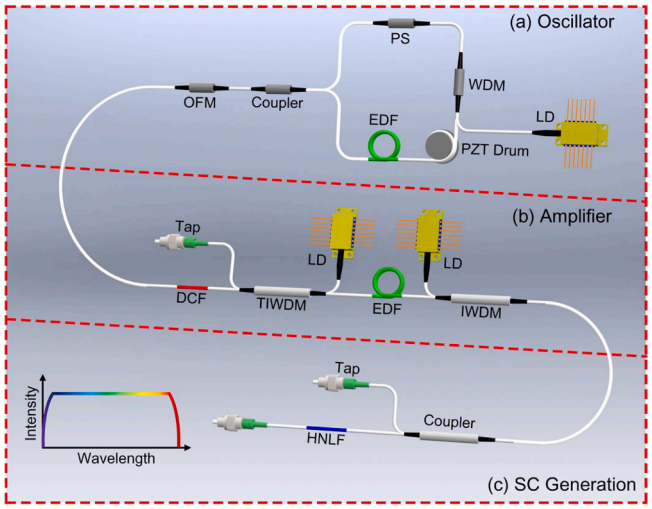

Fig. 1. Schematic diagram of the all-PM fiber laser system. It consists of (a) a figure-9 fiber oscillator, (b) PM DCF assisted one-stage amplifier, (c) single mode PM fiber compressor and supercontinuum (SC) generation part. LD: laser diode, PS: phase shifter, WDM: wavelength division multiplexer, PZT Drum: piezoelectric transducer driven, drum like mechanical unit, OFM: optical fiber mirror, EDF: erbium-doped fiber, DCF: dispersion-compensating fiber, TIWDM: tap, isolator WDM hybrid, IWDM: isolator WDM hybrid, HNLF: highly-nonlinear fiber.

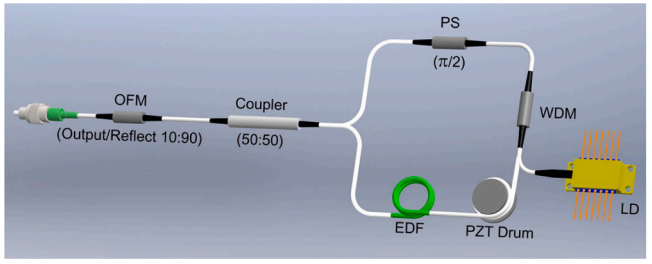

Fig. 2. Schematic diagram of all-PM figure-9 mode-locked Er:fiber oscillator. LD: laser diode, PS: phase shifter, WDM: wavelength division multiplexer, PZT Drum: piezoelectric transducer driven, drum like mechanical unit, OFM: optical fiber mirror, EDF: erbium-doped fiber with a peak core absorption of 96 dB/m at 1530 nm.

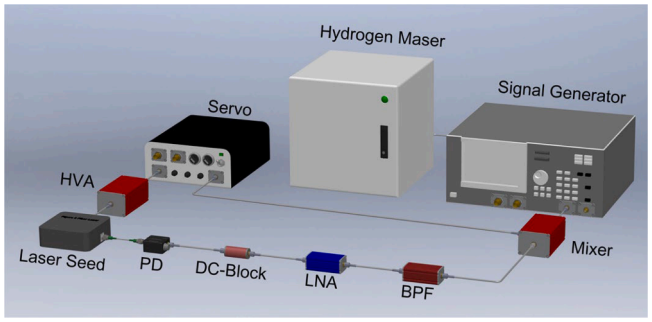

Fig. 3. Phase locked loop for repetition frequency locking. HVA: high voltage amplifier, PD: photodetector, LNA: low noise amplifier, BPF: band pass filter.

In this paper, we focus on the implementation and noise characterization of an all-PM fiber integrated NALM mode-locked Er:fiber laser with hundred-level MHz high repetition rate. Explicitly, our laser system included an all-PM figure-9 mode-locked fiber oscillator, PM-DCF assisted one-stage amplifier and the following PM-SMF compressor. The oscillator delivered 103.4-MHz mode locked femtosecond pulses. The average output power, 3-dB spectral bandwidth and pulse duration were 6.82 mW, 20.57 nm and 189 fs, respectively. 0.0056% [1 Hz, 1 MHz] integrated amplitude (AM) noise at the fundamental repetition rate and 63.7-fs timing jitter [100 Hz, 1 MHz] were characterized. The seed pulses were then pre-chirped by a short length of PM-DCF with positive dispersion and amplified in an EDF amplifier with bidirectional pumping configuration. An average output power of 199 mW corresponding to 1.92-nJ pulse energy was obtained. At last, 48.2 fs compressed pulse with a high peak power of approximate 21 kW was realized by propagating the amplified pulse in a piece of PM SMF with negative GVD and an optimum length of 145 cm. At last, as a proof of the system performance, we also injected the compressed pulse into 38-cm long PM HNLF and broadband SC covering from 950 nm to 2150 nm was generated.

2. Construction of pulse amplification system

The all-PM femtosecond fiber laser system consists of three parts, including a figure-9 mode-locked fiber oscillator, a nonlinear CPA [43–46] and a PM-SMF compressor, as illustrated in Fig. 1. The all-PM fiber and fiber components integrated structure ensures a good environmental stability. In the following of this section, we will discuss the PM fiber laser system in details according to the function of each part.

2.1. Principle and fabrication of figure-9 fiber laser and the stabilization of the repetition frequency

The schematic diagram of figure-9 mode-locked all-PM fiber laser is shown in Fig. 2. It is composed of a NALM loop and a linear arm. In NALM loop, the gain medium is ~28-cm long PM EDF (*n*LIGHT, Er80-4/125-HD-PM, peak core absorption of 96 dB/m @1530 nm). The pump light provided by a 980 nm laser diode (LD) is coupled into the NALM loop through a reflection-type 980/1550 nm WDM. A PS is adopted to induce an π/2 phase difference between the clockwise and counter-clockwise propagated light in the NALM loop and thus initiate the mode locking operation at a relative high repetition rate, around 100 MHz for example. The linear arm is fabricated by ~35-cm long standard Panda-type PM SMF (Nufern, PM1550-XP) and an optical fiber mirror (AFR-PMOFM, 90:10) with an output ratio of 10%. Note that all fiber components used to build the oscillator are PM type.

The repetition frequency of the oscillator is always disturbed by the ambient temperature variation. Both the changes of the intracavity geometric fiber length and the effective refractive index due to the material thermal expansion and thermal optic effects could result to a drift of the repetition frequency. Therefore, a careful temperature control of the oscillator is usually required for the active control and stabilization of the repetition frequency. However, this will inevitably make the whole system more complex and increase the electrical power consumption resulted from the requirement of an additional temperature sensing and control module. Instead, a frequency actuator is often required to regulate the repetition frequency by stretching a section of the intracavity fiber. Although some research groups [47,48] have reported the repetition frequency stabilization method based on the refractive index regulation by adjusting the pump power of the oscillator. This all-optical scheme shows a large bandwidth but also has an evident drawback of small tuning range and an additional pump laser diode is often required. Here, in order to realize a high repetition frequency and simultaneously lock the repetition frequency, we design a repetition frequency actuator based on a PZT-driven, drum like mechanical unit. Around 23-cm passive fiber in the oscillator can be wound on the mechanical unit.

The phase locked loop circuit we adopted to stabilize the repetition frequency is shown in Fig. 3. A small part of the oscillator output laser light with a power of 186.6 μW was detected and converted into an electrical signal through a 3-GHz bandwidth InGaAs photodetector (PD). After the power amplification of the radio frequency (RF) through a low

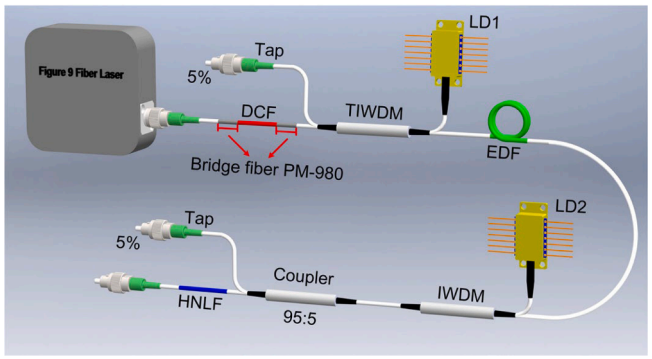

Fig. 4. Schematic diagram of the compact all-PM fiber amplifier, compressor and SC generation system. PM-980: Panda style PM SMF with an operating wavelength covering from 970 nm to 1550 nm, LD: laser diode, EDF: erbium-doped fiber with a peak core absorption of 72 dB/m at 1530 nm, TIWDM: tap, isolator wavelength division multiplexer (WDM) hybrid, IWDM: isolator WDM hybrid, HNLF: highly-nonlinear fiber.

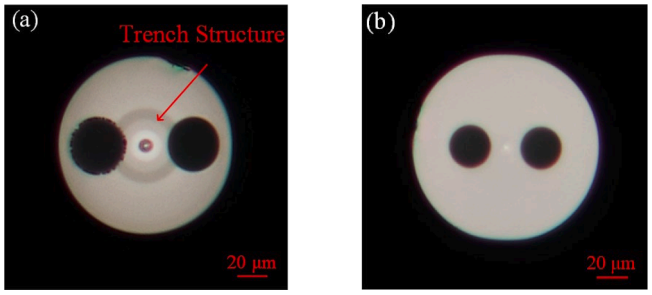

Fig. 5. The end face images of (a) PM-DCF and (b) Er80-4/125-HD-PM EDF that were captured by using a microscope (magnification: ≥300, resolution: <0.6 μm).

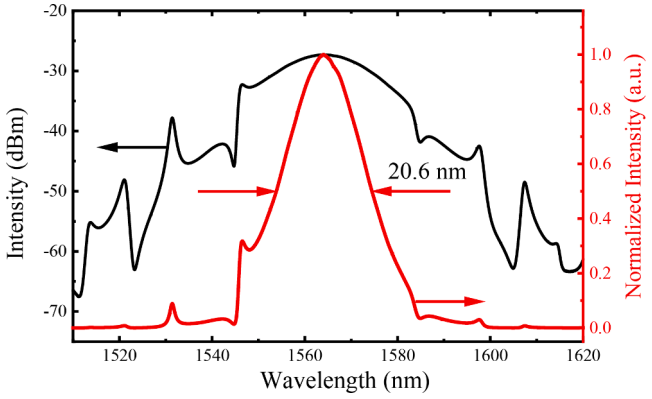

Fig. 6. Optical spectrum of the mode-locked figure-9 fiber oscillator. The 3-dB spectral bandwidth is indicated by two red arrows in the figure. (For interpretation of the references to colour in this figure legend, the reader is referred to the web version of this article.)

noise amplifier and repetition frequency filtering via a low pass filter, an error signal was obtained by mixing the output electrical signal of the low pass filter with the RF reference signal output from an analog signal generator (Agilent Technologies, E8257D) which was calibrated by a hydrogen maser (iMaser 3000). By processing the input error signal, the servo (New Focus, LB1005) system could output a voltage control signal. This voltage signal was then amplified through a 20 × high voltage amplifier and adopted to drive the PZT located in the repetition frequency actuator. The repetition frequency was eventually locked and

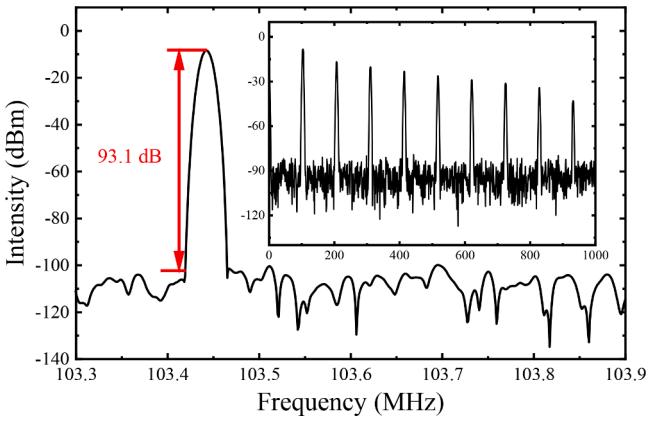

Fig. 7. RF spectrum of the mode-locked pulse train of figure-9 fiber laser. Inset: broadband RF spectrum corresponding to a frequency span of 1000 MHz. The adaptive settings of resolution bandwidth (RBW) and video bandwidth (VBW) were used. (RBW: 200 Hz/3 MHz (inset), VBW: 500 Hz/10 MHz (inset)).

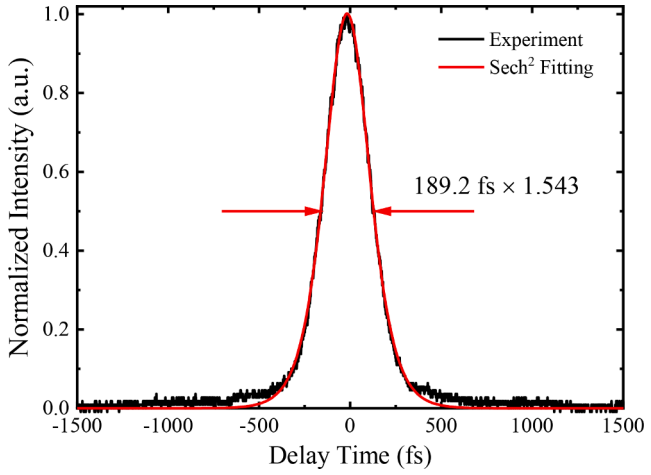

Fig. 8. Pulse autocorrelation trace of the figure-9 all-PM fiber laser.

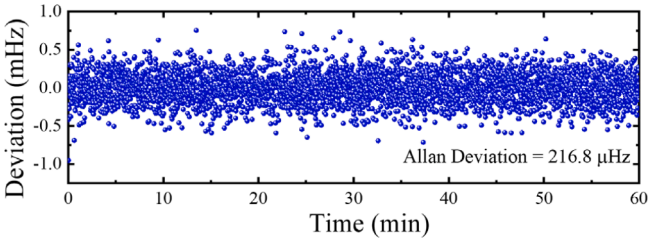

Fig. 9. The fluctuation of the fundamental repetition frequency f_r after locking. The gate time of the frequency counter was set as 1 s and the total recording time was 60 min.

the frequency stability was optimized by carefully tuning the servo control parameters.

2.2. Principle and fabrication of all-PM fiber amplifier

To boost the average output power of the figure-9 oscillator and obtain an even shorter compressed pulse duration, we further designed and built a compact all-PM nonlinear CPA system, as shown in Fig. 4. The same to the oscillator, all the fibers and fiber components were also PM type. The seed pulse from the figure-9 oscillator was first stretched by a segment of DCF. Then, the stretched pulse was amplified by the one-

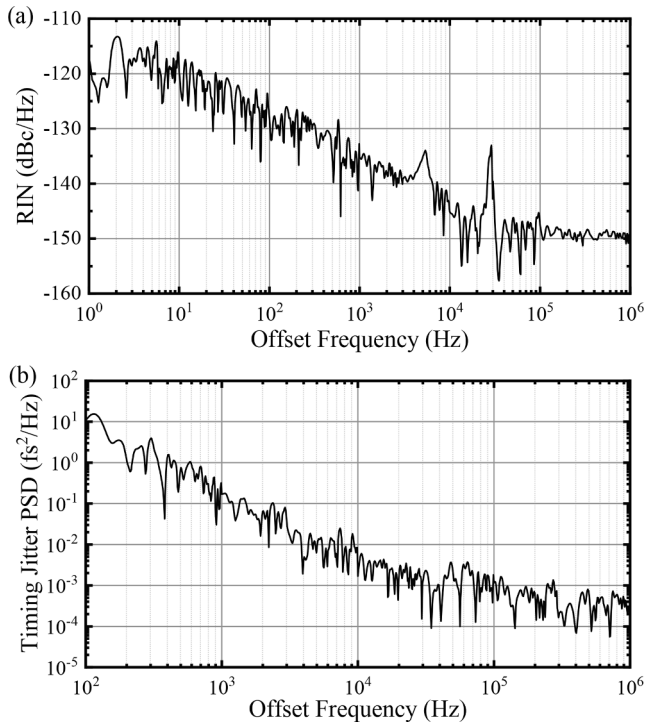

Fig. 10. Single-sideband noise power spectral density (PSD) measurement results. (a) RIN noise at the fundamental repetition frequency. (b) Timing jitter PSD spectrum.

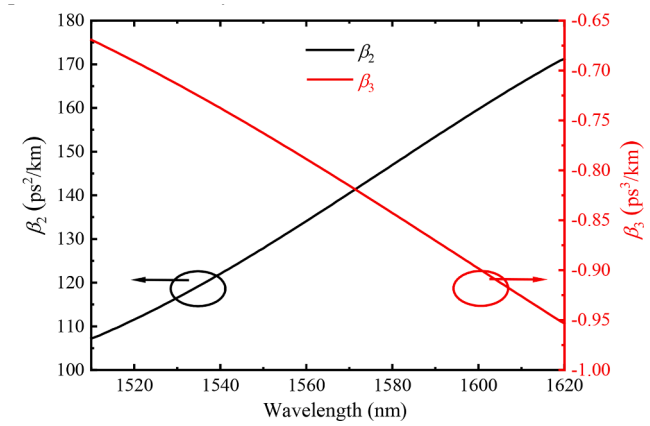

Fig. 11. GVD and TOD curves of PM-DCF.

stage EDF amplifier with a bidirectional pump configuration. The pump light delivered by two single mode 976 nm LDs was launched into the amplifier through two WDMs. The amplified pulse was eventually compressed by splicing a suitable length of PM SMF with negative GVD to the pigtail fiber of the amplifier. Finally, as a performance proof of our all-PM fiber laser system, the compressed pulse was injected into a short piece of HNLF and a broad coherent SC was generated. The typical parameters of the PM fibers used in the laser system present in Fig. 4 will be discussed in detail below.

Explicitly, the output pulses from the figure-9 oscillator were firstly injected into ~68-cm long PM-DCF (Thorlabs PM-DCF, $D = -100 \pm 10$ ps/nm/km, represented by the red line in Fig. 4). Secondly, the stretched pulses were amplified by ~140-cm long PM-EDF (*n*LIGHT, Er80-4/125-HD-PM, $D = -12$ to -18 ps/nm/km, peak core absorption is 72 dB/m @1530 nm, exhibited with the green line in Fig. 4) based amplifier. The tap port of the PM tap, isolator WDM (PM-TIWDM) component reflected

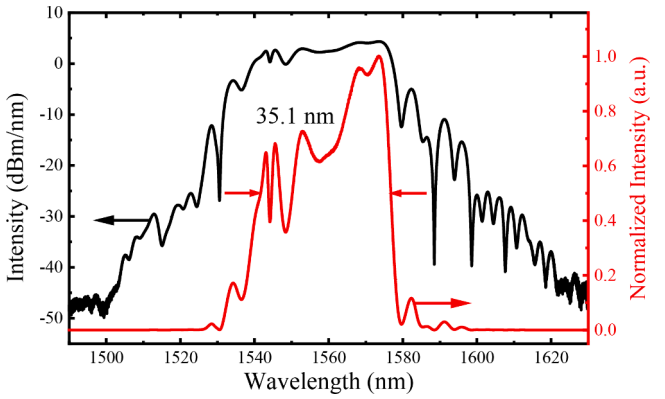

Fig. 12. Optical spectrum of the amplified pulse in logarithmic coordinate (black line) and linear coordinate (red line). (For interpretation of the references to colour in this figure legend, the reader is referred to the web version of this article.)

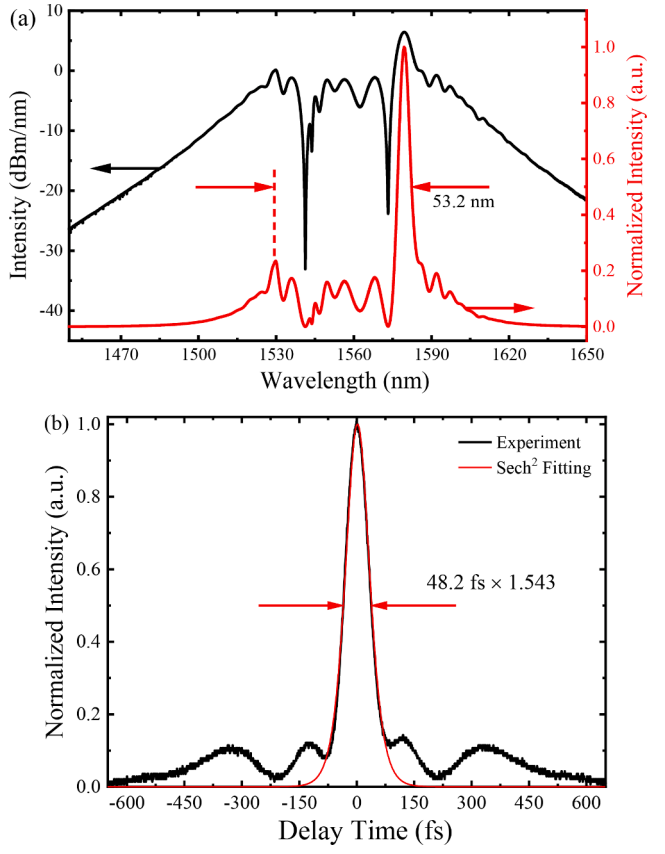

Fig. 13. (a) Optical spectrum in logarithmic coordinate (black line) and linear coordinate (red line) and (b) the autocorrelation trace of the compressed pulse. (For interpretation of the references to colour in this figure legend, the reader is referred to the web version of this article.)

around 5% of the incident power. The reflected light was used to monitor the mode-locked spectrum and detect the repetition frequency. The compact PM isolator WDM (PM-IWDM) was a hybrid fiber component which consisted of a WDM and an isolator. Thirdly, the amplified pulses with positive chirp were coupled into a piece of Panda-type PM SMF (Nufern, PM1550-XP, D = 17 ps/nm/km @1550 nm, shown as the white line in Fig. 4). The pulse duration was compressed almost to the Fourier-transform-limit value by carefully optimizing the length of PM SMF. Finally, the compressed pulses with high peak powers

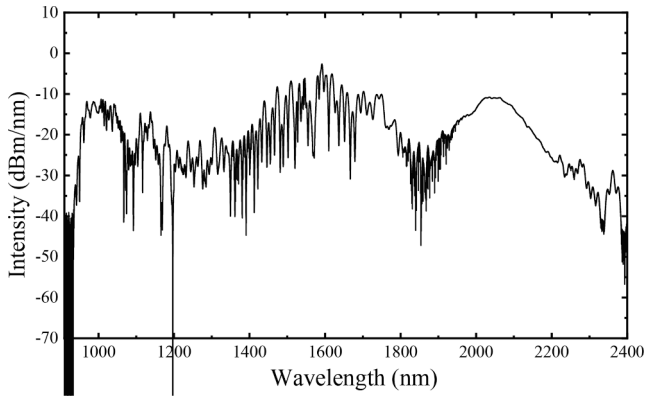

Fig. 14. The supercontinuum generated by injecting the compressed pulse into ~38-cm long PM HNLF.

were directly injected into a 38-cm long PM-HNLF (OFS, $D = -1.5$ to $+2.0$ ps/nm/km, $\gamma = 10.7$ W^{-1}/km, displayed as the blue line in Fig. 4) for the SC generation. An octave-spanning coherent SC was eventually observed. Note also that all the pigtails of the fiber components were the same Panda-type PM1550 SMFs.

As all the fibers in the laser system were PM type, we used a commercial fusion splicer (Fujikura, FSM-100P+) to perform and optimize the splicing processes. End-face images of the PM-DCF and Er80-4/125-HD-PM EDF are shown in Fig. 5. As shown in Fig. 5(a), the cladding of PM-DCF is composed by a ring of highly fluorine doped trench which is different from that of PM1550-XP SMF. Meanwhile, according to the fiber datasheets, the mode field diameter (MFD) of PM-DCF is only 5 μm which is much smaller than that of PM1550-XP SMF (MFD = 10.1 ± 0.4 μm@1550 nm). The large MFD mismatch can result to a large splicing loss. Explicitly, up to 1 dB direct splicing loss between PM1550-XP SMF and PM-DCF is provided by the datasheet. Indeed, we also measured a high splicing loss of 1.2 dB splicing loss between these two kinds of fibers in the process of experiment. Moreover, high fusion current and long discharge time will also make fluorine diffuses rapidly and distort the index profile, which then directly affects the dispersion and mode distribution of the fusion point and introduces an additional fusion loss [49]. Instead, the PM-DCF was not directly spliced with the PM1550-XP SMF and a bridge fiber (Nufern, PM980-XP) with a small core diameter of 5.5 μm was introduced. The splicing loss was reduced from the initial 1.2 dB down to 0.66 dB by careful and repeated optimization of the fusion current, fiber overlap and discharge time parameters. For the splicing between Er80-4-125-HD-PM EDF and PM1550-XP SMF, the standard PM1550-XP SMFs splicing procedure was adopted. The end-face was shown in Fig. 5(b) of which MFD was 6.5 ± 1.0 μm@1550 nm. It should be noted that a high cleaved quality must be ensured to minimize the deformation of the fiber endface and thus the splicing loss. In addition, for the splicing between PM1550-XP SMF and PM-HNLF, an optimized average loss of 0.43 dB for each splicing point at 1560-nm wavelength was obtained by using the same fusion optimization method.

3. Results and discussions

As is well known that the total net cavity dispersion is the main concern parameter for a mode-locked fiber laser. According to the fiber parameter menus, the Er80-4/125-HD-PM EDF shows a positive GVD of 0.02804 ps^2/m and the passive PM1550-XP SMF has a negative GVD of −0.02167 ps^2/m at 1550-nm wavelength. We thus estimated a net cavity dispersion of about −0.02 ps^2. Considering both the positive and negative dispersion optical fibers were used in the cavity, as a result, the mode-locked fiber laser was operated in the stretched-pulse regime. In the experiment, an optical spectrum analyzer (YOKOGAWA, AQ6370D) with the minimum resolution of 20 pm was utilized to measure the output spectrum, as shown in Fig. 6. At a pump current of 460 mA, the central wavelength and 3-dB spectral width were measured as 1562 nm and 20.6 nm, respectively.

We also measured the RF spectum of the mode-locked pulse train by using an InGaAs PD with 3-GHz bandwidth and a phase noise analyzer (Rohde & Schwarz, FSWP50), as shown in Fig. 7. The RF spectrum of the fundamental repetition frequency exhibited a central frequency of 103.44 MHz and a signal to noise ratio of up to ~93 dB.

For the pulse width measurement, an intensity autocorrelator (Femto-chrome, FR-103MN) based on the second-harmonic generation (SHG) process was used to measure the intensity autocorrelation trace, as shown in Fig. 8. A pulse duration of 189 fs was measured by assuming a sech^2 pulse profile. The time-bandwidth product was calculated as 0.477 indicating the output pulse was still negatively chirped. In addition, for a pump current of 650 mA, an average output power of 6.82 mW was measured by an optical power meter (JDSU, OLP-85).

The fundamental repetition rate (f_r) of the figure-9 oscillator was also locked by using the phase locked loop described in Section 2. The fluctuation of f_r frequency after locking was monitored by using a frequency counter (Keysight, 53230A) with a gate time of 1 s. The Allan deviation was calculated as 216.8 μHz based on the recorded f_r data with a total lasting time of 60 min, as displayed in Fig. 9. This corresponded to an in-loop relative frequency stability of 2.1×10^{-12}.

To evaluate the noise properties of our figure-9 fiber laser, we further measured the amplitude noise or RIN at the fundamental repetition rate and phase noise at the fifth-order harmonic frequency of around 517 MHz, as shown in Fig. 10. A PD (Thorlabs, DET08CFC, 5-GHz bandwidth, no amplifier) powered by a 12 V dry battery was adopted to convert the laser pulses output from the tap port of PM-TIWDM into an electrical signal. The phase noise analyzer (Rohde & Schwarz, FSWP50) was then used to measure the RIN and phase noise. The noise measurement method we adopted was similar to that reported in [17]. For RIN measurement, the phase noise analyzer was set to AM mode (correlation factor: 50), and the measured single-sideband PSD curve of AM noise is shown in Fig. 10(a). For a pump current of 550 mA, the rms RIN value was 0.0056% at the offset frequency range of 1 Hz to 1 MHz. An overshoot can be clearly seen from the RIN PSD curve at an offset frequency of around 5 kHz. The occurrence of this noise spectral peak results from the finite upper-state lifetime of the Er gain medium and the resonant relaxation oscillation process. As shown in the figure, at 1-kHz offset frequency, the RIN spectrum shows a PSD of around −135 dBc/Hz. For offset frequencies lower than 1 kHz, the RIN PSD drops with ~10 dB/decade slope. In addition, according to the RIN measurement results of the pump laser, the evident noise spikes at around 30 kHz originates from the pump technical noise. Above the relaxation oscillation frequency, the RIN quicky decays and approaches a noise floor of around −148 dBc/Hz. The noise floor determined by the vacuum fluctuation or shot noise which arises from the oscillator output coupler can be calculated by Eq. (1). The parameters h, v_c and P_{avg} represent the Plank constant, the center optical frequency and the average output power from the output coupler [50,51]. For a pump current of 550 mA, which corresponds to an output power of around 6.2 mW, the shot noise-limited RIN-PSD floor is about −164 dBc/Hz. Meanwhile, the RIN-PSD floor corresponds to the PD shot noise can be calculated by Eq. (2). q and I_0 represent the charge of an electron and the photocurrent converted by PD. Explicitly, considering an input power of 186.6 μW and a responsivity of 1.0 A/W, the RIN-PSD floor set by the PD shot noise is calculated as −148 dBc/Hz. The noise PSD values at offset frequencies above 100 kHz accords well with the RIN-PSD floor induced by PD shot noise. This indicates that the RIN measurement above 100-kHz Fourier frequencies are limited by the PD shot noise. In addition, according to [50], for fundamental repetition frequency, part of intensity noise could be coupled to phase noise, so we measured the phase noise PSD spectrum of the fifth-order harmonic of the fundamental repetition rate in the experiment. Fig. 10(b) shows the timing jitter PSD spectrum. The integrated timing jitter for an offset frequency interval [100 Hz–1 MHz]

Table 1
Representative performances of free-running figure-9 mode-locked fiber lasers.

Laser System Structure	Repetition Frequency (MHz)	Cavity Dispersion (ps^2)	Pulse Width (fs)	Integrated rms RIN (%)	Integrated Timing Jitter (fs)	Measurement Method	Refs.
Figure-9 Er: fiber laser							
All-PM fiber integrated							
All-PM fiber integrated oscillator, amplifier and compressor	103.4	−0.02	48.2	0.0056 [1 Hz, 1 MHz]	63.7 [100 Hz, 1 MHz]	PD	Our work
All-PM fiber oscillator with optical bandpass filters	35.67	−0.12	N/A	0.0054 [10 Hz, 1 MHz]	2.95 [10 kHz,1 MHz]	BOC	[52]
All-PM fiber oscillator	121	−0.015	477	N/A	N/A	N/A	[30]
All-PM fiber oscillator, amplifier and compressor	64.7	~−0.055	28	N/A	N/A	N/A	[29]
All-PM fiber oscillator based on a hybrid fiber component	201.14	−0.012	510	N/A	N/A	N/A	[32]
Spatial optical path included							
PM fiber components, PBS splitter, spatial phase shifter and spatial optical path based linear arm part	250	Near zero	N/A	~0.005 [1 Hz, 1 MHz]	N/A	N/A	[28]
All-PM fiber integrated NALM loop and spatial optical path based linear arm part	122	−0.0107	157	0.004 [100 Hz, 1 MHz]	1.85 [10 kHz, 1 MHz]	BOC	[53]
			108	0.76 [100 Hz, 1 MHz]	1.91 [10 kHz, 1 MHz]		
PM fiber coupler, spatial phase shifter in the NALM ring and spatial optical path based linear arm part	72	Near zero	N/A	N/A	0.04 [10 kHz, 10 MHz]	BOC	[27]
Figure-9 Yb: fiber laser							
All-PM fiber integrated NALM ring, spatial phase shifter, and spatial optical path based linear arm part, grating-pair adopted for dispersion compensation	78.25	−0.03	N/A	0.028 [1 Hz, 1 MHz]	803 [100 Hz, 1 MHz]	PD	[17]
	78.30	−0.015		0.019 [1 Hz, 1 MHz]	351 [100 Hz, 1 MHz]		
	78.45	+0.015		0.048 [1 Hz, 1 MHz]	202 [100 Hz, 1 MHz]		
	78.45	Near zero		0.006 [1 Hz, 1 MHz]	81 [100 Hz, 1 MHz]		
	78.50	Near zero		0.003 [1 Hz, 1 MHz]	72 [100 Hz, 1 MHz]		
All-PM fiber and fiber components integrated	54	−0.01	88	0.0255 [10 Hz, 1 MHz]	0.7 [25 kHz, 5 MHz]	BOC	[33]
NALM loop contains a spatial phase bias module and spatial optical path based linear arm part, a grating-pair adopted for dispersion compensation	~131	N/A	~80	0.18 [1 Hz, 1 MHz]	N/A	PD	[54]
PM fiber components with spatial phase shifter and linear cavity	700	−0.016	215	0.015 [10 Hz, 10 MHz]	21 [100 kHz, 10 MHz]	PD	[55]
			325	0.016 [10 Hz, 10 MHz]	21 [100 kHz, 10 MHz]		

was 63.7 fs.

$$S_{RIN}^{shot\ \ noise}(f) = \frac{2h\nu_c}{P_{avg}} \tag{1}$$

$$S_{RIN}^{shot}(f) = \frac{2q}{I_0} \tag{2}$$

Next, in terms of all-PM fiber amplifier construction, our main concerns include two aspects. On one hand, compared with the width of the oscillator output pulse, to obtain an even shorter pulse duration after compression, we have to broaden the spectrum bandwidth based on the nonlinear self-phase modulation (SPM) effect during pulse amplification and compression processes. To achieve this goal, a proper pulse stretching ratio and an initial positive pulse chirp are critical. Because, for an input negatively chirped pulse, the SPM induced positive chirp will be cancelled out due to the destructive interference processes. On the other hand, the PM-DCF exhibits a large positive GVD, e. g. $\beta_2 = 133.5\ ps^2/km$ and a negative TOD coefficient of $\beta_3 = -0.79\ ps^3/km$ at 1560-nm wavelength, as shown in Fig. 11. This dispersion characteristic enables us to achieve a large pulse broadening factor by using a short piece of PM-DCF. More importantly, the negative TOD can be adopted to compensate the positive TOD of EDF and passive PM1550-XP SMFs and thus can greatly improve the compressed pulse quality.

Experimentally, after propagating in 68-cm long PM-DCF, the duration of the positively chirped pulse was measured as 1.06 ps. Bidirectional pump scheme was adopted to ensure a uniform small signal gain along the entire amplifier length and effectively avoiding the occurrence of gain narrowing process. The spectral bandwidth was

broadened from 20.6 nm to 35.1 nm after amplification. As shown in the Fig. 12, the intensity of the Kelly sideband with a center wavelength of around 1531 nm was not boosted dramatically due to an initial low power and high absorption coefficient, e. g., 80 ± 20 dB/m of the Er80-4/125-HD-PM EDF at 1530-nm wavelength. It should also note that, the optical power was not concentrated on the central spectral components around 1560 nm. Instead, the spectrum extended to both the short and long wavelength sides and spectral modulation resulted from the nonlinear SPM process can be clearly seen.

The amplified pulse was then compressed by propagating the pulse train in a piece of PM1550-XP SMF. Cutback method was adopted to optimize the fiber length according to the measured intensity autocorrelation trace of the compressed pulse. At an output power of 199 mW corresponding to a forward pump power of 490 mW and backward pump power of 435 mW, the measured optical spectrum and autocorrelation trace of the compressed pulse are shown in Fig. 13. The optimized length of PM1550-XP SMF was ~145 cm. Due to the strong SPM effect resulted from the high average power and the quickly increased peak power in the process of pulse compression, the optical spectrum of the compressed pulse exhibited multiple spectral peaks and a broad spectral range covering from ~1515 nm to ~1605 nm. Fig. 13(b) exhibits the autocorrelation trace of the compressed pulse and according to the good fitting result based on $sech^2$ pulse profile, a compressed pulse duration of as short as 48.2 fs was experimentally obtained. Two sidelobes with low intensities which symmetrically located on both sides of the autocorrelation trace could also be observed. After an integral calculation, the ratio between the area of the central part to that of the whole autocorrelation trace was around 54%. We thus estimated a pulse peak power of ~21 kW relating to the compressed pulse.

4. Application

As a performance proof of our all-PM fiber laser system, we further injected the compressed pulse into 38-cm long PM-HNLF and observed the generated SC, as shown in Fig. 14. The spectrum covered from ~950 nm to ~2150 nm with a spectral range larger than one octave. The generated coherent SC can be further applied to detect the CEO signal in a fiber frequency comb system.

5. Conclusion

In summary, we have presented a compact and robust femtosecond fiber laser system based on an all-PM fiber and fiber components integrated structure. At the fundamental repetition rate of 103.4 MHz, the RF spectrum of the figure-9 oscillator exhibited a high signal-to-noise ratio of up to 93.1 dB. In addition, the rms RIN over a large offset frequency range of 1 Hz to 1 MHz was only 0.0056% which is in the ranks of ultralow amplitude noise fiber lasers. The integrated timing jitter was measured as 63.7 fs ([100 Hz, 1 MHz]). Meanwhile, a relative f_r stability of 2.1×10^{-12} at 1-s gate time was obtained by using a self-designed frequency actuator. The output average power of 6.82 mW was successively amplified to 199 mW via PM-DCF assisted one-stage all-PM fiber based nonlinear CPA with a bidirectional pump structure. Benefitting from the large positive GVD and a negative TOD around 1560-nm wavelength, 48.2-fs compressed pulse duration with ~21 kW pulse peak power was eventually obtained. A coherent and broadband SC covering from ~950 nm to ~2150 nm was also generated by pumping 38-cm long PM-HNLF with the compressed pulses. For comprehensive comparisons, Table 1 summarizes the representative and state of the art performances of figure-9 Er: and Yb: fiber lasers mode-locked by NALM. As shown in the Table, for the first time, we gave a full characterization of the noise performance of a NALM based figure-9 Er:fiber laser with an all-PM fiber integrated structure and 100-MHz-level high repetition rate. In the future work, we will focus on the optimization of the net cavity dispersion to around zero which can help to further reduce the timing jitter. Detection of CEO frequency, constructions and applications of low noise all-PM fiber OFC is also an important research work to be carried out.

CRediT authorship contribution statement

Haihao Cheng: Conceptualization, Methodology, Formal analysis, Writing – original draft. **Zhao Zhang:** Investigation, Validation. **Ran Pan:** Resources, Validation. **Ting Zhang:** Investigation, Validation. **Ye Feng:** Resources, Validation. **Xiaohong Hu:** Data curation, Formal analysis, Writing – original draft, Writing – review & editing, Project administration. **Yishan Wang:** Supervision, Project administration, Funding acquisition. **Shun Wu:** Validation, Funding acquisition.

Declaration of Competing Interest

The authors declare that they have no known competing financial interests or personal relationships that could have appeared to influence the work reported in this paper.

Data availability

Data will be made available on request.

Acknowledgements

This work is supported by grants from Western Young Scholars Program of CAS (XAB2020YN11), Natural Science Foundation of China (NSFC) (61875227) and the Open Research Fund of State Key Laboratory of Transient Optics and Photonics (SKLST202105).

References

[1] W.J. Yang, P.G. Kazansky, Y.P. Svirko, Non-reciprocal ultrafast laser writing, Nat. Photonics. 2 (2) (2008) 99–104, https://doi.org/10.1038/nphoton.2007.276.
[2] K. Sugioka, Y. Cheng, Ultrafast lasers-reliable tools for advanced materials processing, Light: Sci. Appl. 3 (2014) e149, https://doi.org/10.1038/lsa.2014.30.
[3] P.S. Binder, Flap dimensions created with the IntraLase FS laser, J. Cataract. Refract. Surg. 30 (1) (2004) 26–32, https://doi.org/10.1016/S0886-3350(03)00578-9.
[4] H.K. Tonshoff, A. Ostendorf, S. Nolte, F. Korte, T. Bauer, Micromachining using femtosecond lasers, Proc. SPIE – Int. Soc. Opt. Eng. 4088 (2000) 136–139, https://doi.org/10.1117/12.405700.
[5] Y. Feng, X. Xu, X.H. Hu, Y.S. Liu, Y.S. Wang, W. Zhang, Z. Yang, L.N. Duan, W. Zhao, Z. Cheng, Environmental-adaptability analysis of an all polarization-maintaining fiber-based optical frequency comb, Opt. Express 23 (13) (2015) 17549–17559, https://doi.org/10.1364/OE.23.017549.
[6] Y.J. Cai, R. Pan, T. Zhang, Y.S. Liu, H.S. Wang, W. Zhang, Y.S. Wang, W. Zhao, Y. Feng, X.H. Hu, Compact, robust, and repetition-ratelocked all-polarization-maintaining femtosecond fiber laser system, Opt. Eng. 58 (4) (2019) 1–7, https://doi.org/10.1117/1.OE.58.4.046108.
[7] H. Carstens, M. Högner, T. Saule, S. Holzberger, N. Lilienfein, A. Guggenmos, C. Jocher, T. Eidam, D. Esser, V. Tosa, V. Pervak, J. Limpert, A. Tünnermann, U. Kleineberg, F. Krausz, I. Pupeza, High-harmonic generation at 250 MHz with photon energies exceeding 100 eV, Optica 3 (4) (2016) 366–369, https://doi.org/10.1364/OPTICA.3.000366.
[8] Z.G. Zhao, Y. Kobayashi, Realization of a mW-level 10.7-eV ($\lambda = 115.6$ nm) laser by cascaded third harmonic generation of a Yb:fiber CPA laser at 1-MHz, Opt. Express 25 (12) (2017) 13517–13526, https://doi.org/10.1364/OE.25.013517.
[9] H.Y. Xu, W. Cao, K. Mi, Y.L. Mo, X. Chen, Q.B. Zhang, P.X. Lu, Direct in situ measurement of an ultrashort pulse using an optical hologram, Phys. Rev. Appl. 17 (2022), 014046, https://doi.org/10.1103/PhysRevApplied.17.014046.
[10] K. Mi, W. Cao, H.Y. Xu, Q.B. Zhang, P.X. Lu, Method for high precision measurement of decaying dynamics using attosecond wave-mixing spectroscopy, Opt. Express 29 (2) (2021) 2798–2808, https://doi.org/10.1364/OE.413829.
[11] J.M. Dudley, G. Genty, S. Coen, Supercontinuum generation in photonic crystal fiber, Rev. Mod. Phys. 78 (4) (2006) 1135–1184, https://doi.org/10.1103/RevModPhys.78.1135.
[12] K.L. Corwin, N.R. Newbury, J.M. Dudley, S. Coen, S.A. Diddams, K. Weber, R. S. Windeler, Fundamental noise limitations to supercontinuum generation in microstructure fiber, Phys. Rev. Lett. 90 (11) (2003), 113904, https://doi.org/10.1103/PhysRevLett.90.113904.
[13] R. Paschotta, Noise of mode-locked lasers (part ii): timing jitter and other fluctuations, Appl. Phys. B-Lasers O. 79 (2) (2004) 163–173, https://doi.org/10.1001/s00340-004-1548-9.

[14] L. Nugent-Glandorf, T.A. Johnson, Y. Kobayashi, S.A. Diddams, Impact of dispersion on amplitude and frequency noise in a Yb-fiber laser comb, Opt. Lett. 36 (9) (2011) 1578–1580, https://doi.org/10.1364/OL.36.001578.

[15] Y.J. Song, K. Jung, J. Kim, Impact of pulse dynamics on timing jitter inmode-locked fiber lasers, Opt. Lett. 36 (10) (2011) 1761–1763, https://doi.org/10.1364/OL.36.001761.

[16] Z, Łaszczych, G, Soboń, Dispersion-tailoring of a NALM-based all-PM Er-doped femtosecond fiber laser, in: 2021 Conference on Lasers and Electro-Optics Europe & European Quantum Electronics Conference (CLEO/Europe-EQEC), 2021, pp. 9542400. https://doi.org/10.1109/CLEO/Europe-EQEC52157.

[17] A.S. Mayer, W. Grosinger, J. Fellinger, G. Winkler, L.W. Perner, S. Droste, S. H. Salman, C. Li, C.M. Heyl, I. Hartl, O.H. Heckl, Flexible all-PM NALM Yb:fiber laser design for frequency comb applications: operation regimes and their noise properties, Opt. Express 28 (13) (2020) 18946–18968, https://doi.org/10.1364/OE.394543.

[18] Y. Ling, Q. Huang, C. Zou, Z. Xing, Z. Yan, C. Zhao, K. Zhou, L. Zhang, C. Mou, L-band ghz femtosecond passively harmonic mode-locked Er-doped fiber laser based on nonlinear polarization rotation, IEEE Photon. J. 11 (4) (2019) 1–7, https://doi.org/10.1109/JPHOT.2019.2927771.

[19] D. Deng, L. Zhan, Z. Gu, Y. Gu, Y. Xia, 55-fs pulse generation without wave-breaking from an all-fiber Erbium-doped ring laser, Opt. Express 17 (6) (2009) 4284–4288, https://doi.org/10.1364/OE.17.004284.

[20] J. Boguslawski, J. Sotor, G. Sobon, K.M. Abramski, 80 fs passively mode-locked Er-doped fiber laser, Laser Phys. 25 (6) (2015), 065104, https://doi.org/10.1088/1054-660X/25/6/065104.

[21] L. Zhou, Y. Liu, G. Xie, W. Zhang, Z. Zhu, C. Ouyang, C. Gu, W. Li, Generation of stretched pulses from an all-polarization-maintaining Er-doped mode-locked fiber laser using nonlinear polarization evolution, Appl. Phys. Express 12 (5) (2019), 052017, https://doi.org/10.7567/1882-0786/ab15c0.

[22] H. Liu, M.-L. Gong, S.-Y. Cao, B.-K. Lin, Z.-J. Fang, A 303 MHz fundamental repetition rate femtosecond Er:fiber ring laser, Acta Phys. Sin. 64 (2015), 114210, https://doi.org/10.7498/aps.64.114210.

[23] D.A. Dvoretskiy, S.G. Sazonkin, I.O. Orekhov, I.S. Kudelin, A.B. Pnev, V.E. Karasik, A.A. Krylov, L.K. Denisov, High-energy ultrashort-pulse all-fiber erbium-doped ring laser with improved free-running performance, J. Opt. Soc. Am. B 35 (8) (2018) 2010–2014, https://doi.org/10.1364/JOSAB.35.002010.

[24] W. Liu, H. Shi, J. Cui, C. Xie, Y. Song, C. Wang, M. Hu, Single-polarization large-mode-area fiber laser mode-locked with a nonlinear amplifying loop mirror, Opt. Lett. 43 (12) (2018) 2848–2851, https://doi.org/10.1364/OL.43.002848.

[25] D. Li, L. Li, J. Zhou, L. Zhao, D. Tang, D. Shen, Characterization and compression of dissipative-soliton-resonance pulses in fiber lasers, Sci. Rep. 6 (2016) 23631, https://doi.org/10.1038/srep23631.

[26] S. Ko, J. Lee, J. Koo, J.-H. Lee, Experimental investigation into generation of bursts of linearly-polarized, dissipative soliton pulses from a figure-eight fiber laser at 1.03 μm, Jpn. J. Appl. Phys. 57 (2018), 032701, https://doi.org/10.7567/JJAP.57.032701.

[27] N. Kuse, J. Jiang, C.C. Lee, T.R. Schibli, M.E. Fermann, All polarization-maintaining Er fiber-based optical frequency combs with nonlinear amplifying loop mirror, Opt. Express 24 (3) (2016) 3095–3102, https://doi.org/10.1364/OE.24.003095.

[28] W. Hänsel, H. Hoogland, M. Giunta, S. Schmid, T. Steinmetz, R. Doubek, P. Mayer, S. Dobner, C. Cleff, M. Fischer, R. Holzwarth, All polarization-maintaining fiber laser architecture for robust femtosecond pulse generation, Appl. Phys. B 123 (41) (2017) 1–6, https://doi.org/10.1007/s00340-016-6598-2.

[29] F.H. Chen, Q. Hao, H.P. Zeng, Optimization of an NALM mode-locked all-pM Er: fiber laser system, IEEE Photonic Tech. L. 29 (23) (2017) 2119–2122, https://doi.org/10.1109/LPT.2017.2765686.

[30] K. Yin, Y.M. Li, Y.B. Wang, X. Zheng, T. Jiang, Self-starting all-fiber PM Er:laser mode locked by a biased nonlinear amplifying loop mirror, Chin. Phys. B 28 (12) (2019), 124203, https://doi.org/10.1088/1674-1056/ab4d42.

[31] Y. Zhou, Y.W. Zeng, J. Yin, T. Dong, L.J. Sun, Y. Zhang, K. Xu, All-polarization-maintaining figure-of-9 soliton and dispersion-managed Er-doped fiber oscillators, Laser Physics 30 (4) (2020), 045101, https://doi.org/10.1088/1555-6611/ab7a99.

[32] Q.H. Deng, K. Yin, J.H. Zhang, X. Zheng, T. Jiang, A 200 MHz Compact Environmentally-stable mode-locked Figure-9 fiber laser, IEEE Photon. J. 13 (4) (2021) 1500605, https://doi.org/10.1109/JPHOT.2021.3095159.

[33] Y.X. Ma, S.H. Salman, C. Li, C. Mahnke, Y. Hua, S. Droste, J. Fellinger, A.S. Mayer, O.H. Heckl, C.M. Heyl, I. Hartl, Compact, all-PM fiber integrated and alignment-free ultrafast Yb:fiber NALM laser with sub-femtosecond timing jitter, J. Lightwave Technol. 39 (13) (2021) 4431–4438, https://doi.org/10.1109/JLT.2021.3070208.

[34] D. Strickland, G. Mourou, Compression of amplified chirped optical pulses, Opt. Commun. 55 (6) (1985) 219–221, https://doi.org/10.1016/0030-4018(85)90151-8.

[35] T. Eidam, J. Rothhardt, F. Stutzki, F. Jansen, S. Haedrich, H. Carstens, C. Jauregui, J. Limpert, A. Tuennermann, Fiber chirped-pulse amplification system emitting 3.8 GW peak power, Opt. Express 19 (1) (2011) 255–260, https://doi.org/10.1364/OE.19.000255.

[36] A. Galvanauskas, Ultrashort pulse fiber amplifiers, Ultrafast Lasers: technology and applications, in: M. Fermann, A. Galvanauskas, G. Sucha (Eds.), Ultrafast Lasers: Technology and Applications, CRC Press, 2002.

[37] W.H. Renninger, F.W. Wise, Fundamental limits to mode-locked lasers: toward terawatt peak powers, IEEE J. Sel. Top. Quant. 21 (1) (2016) 1100208, https://doi.org/10.1109/JSTQE.2014.2329936.

[38] L. Shah, M.E. Fermann, High-power ultrashort-pulse fiber amplifiers, IEEE J. Sel. Top. Quant. 13 (3) (2007) 552–558, https://doi.org/10.1109/JSTQE.2007.896096.

[39] D.G. Purdie, D. Popa, V.J. Wittwer, Z. Jiang, G. Bonacchini, F. Torrisi, S. Milana, E. Lidorikis, A.C. Ferrari, Few-cycle pulses from a graphene mode-locked all-fiber laser, Appl. Phys. Lett. 106 (25) (2015), 253101, https://doi.org/10.1063/1.4922397.

[40] J. Yu, Y. Feng, Y.J. Cai, X.H. Li, X.H. Hu, W. Zhang, L.N. Duan, Z. Yang, Y.S. Wang, Y.S. Liu, W. Zhao, 34-fs, all-fiber all-polarization-maintaining single-mode pulse nonlinear amplifier, Opt. Express 24 (15) (2016) 16630–16637, https://doi.org/10.1364/OE.24.016630.

[41] H. Luo, L. Zhan, L. Zhang, Z.Q. Wang, C.X. Gao, X. Fang, Generation of 22.7-fs 2.8-nJ pulses from an erbium-doped all-fiber laser via single-stage soliton compression, J. Lightwave Technol. 35 (17) (2017) 3780–3784, https://doi.org/10.1109/JLT.2017.2723088.

[42] Z.R. Guo, Q. Hao, J.S. Peng, H.P. Zeng, Environmentally stable er-fiber mode-locked pulse generation and amplification by spectrally filtered and phase-biased nonlinear amplifying long-loop mirror, High Power Laser SCI 7 (3) (2019) e47.

[43] L. Kuznetsova, F. Wise, Scaling of femtosecond Yb-doped fiber amplifiers to tens of microjoule pulse energy via nonlinear chirped pulse amplification, Opt. Lett. 32 (18) (2007) 2671–2673, https://doi.org/10.1364/OL.32.002671.

[44] M. Hanna, D. Papadopoulos, F. Druon, P. Georges, Distributed nonlinear fiber chirped-pulse amplifier system, Opt. Express 17 (13) (2009) 10835–10840, https://doi.org/10.1364/OE.17.010835.

[45] H.L. Yu, P.F. Zhang, X.L. Wang, P. Zhou, J.B. Chen, High-Average-Power Polarization Maintaining All-Fiber-Integrated Nonlinear Chirped Pulse Amplification System Delivering Sub-400 fs Pulses, IEEE Photonics J. 8 (2) (2016) 7100507, https://doi.org/10.1109/JPHOT.2016.2547330.

[46] R.C. Lü, H. Teng, J.F. Zhu, Y. Yu, W. Liu, G.Q. Chang, Z.Y. Wei, High power Yb-fiber laser amplifier based on nonlinear chirped-pulse amplification at a repetition rate of 1 MHz, Chin. Opt. Lett. 19 (9) (2021), 091401, https://doi.org/10.3788/COL202119.091401.

[47] S. Rieger, T. Hellwig, T. Walbaum, C. Fallnich, Optical repetition rate stabilization of a mode-locked all-fiber laser, Opt. Express 21 (4) (2013) 4889–4895, https://doi.org/10.1364/OE.21.004889.

[48] K. Yang, Q. Hao, H. Zeng, All-optical high-precision repetition rate locking of an Yb-doped fiber laser, IEEE Photon. Technol. Lett. 27 (8) (2015) 852–855, https://doi.org/10.1109/LPT.2015.2398031.

[49] L. Grüner-Nielsen, T. Geisler, J. Fini, M. F. Yan, P. W. Wisk, B. Mangan, E. M. Monberg, Polarization maintaining dispersion compensating fiber, in: 2014 European Conference on Optical Communication (ECOC) (2014) https://doi.org/10.1109/ECOC.2014.6963856.

[50] J. Kim, Y. Song, Ultralow-noise mode-locked fiber lasers and frequency combs: principles, status, and applications, Adv. Opt. Photonics 8 (3) (2016) 465–540, https://doi.org/10.1364/AOP.8.000465.

[51] A. Sennaroglu, Solid-State Lasers and Applications, Optical Science and Engineering, CRC Press, Florida, 2007.

[52] D. Kim, S.Y. Zhang, D. Kwon, R.Y. Liao, Y.F. Cui, Z.G. Zhang, Y.J. Song, J. Kim, Intensity noise suppression in mode-locked fiber lasers by double optical bandpass filtering, Opt. Lett. 42 (20) (2017) 4095–4098, https://doi.org/10.1364/OL.42.004095.

[53] Y.H. Pi, H.C. Tian, R.M. Li, Y. Han, Y.J. Song, M.L. Hu, Timing Jitter and Intensity Noise Characterization of a 122-MHz All-PM NALM Mode-Locked Fiber Laser, IEEE Photon. Technol. Lett. 33 (24) (2021) 1439–1442, https://doi.org/10.1109/LPT.2021.3125994.

[54] Y.H. Li, N. Kuse, A. Rolland, Y. Stepanenko, C. Radzewicz, M.E. Fermann, Low noise, self-referenced all polarization maintaining Ytterbium fiber laser frequency comb, Opt. Express 25 (15) (2017) 18017–18023, https://doi.org/10.1364/OE.25.018017.

[55] G.Y. Liu, X.H. Jiang, A.M. Wang, G.Q. Chang, F. Kaertner, Z.G. Zhang, Robust 700 MHz mode -locked Yb:fiber laser with a biased nonlinear amplifying loop mirror, Opt. Express 26 (20) (2018) 26003–26009, https://doi.org/10.1364/OE.26.026003.